Science and Technology Indonesia
e-ISSN:2580-4391 *p*-ISSN:2580-4405
Vol. 9, No. 2, April 2024

Research Paper

Synthesis of a 3D Porous Multicomponent Bioceramic Scaffold

Yessie Widya Sari[1]*, Ryaas Mishbachul Munir[1], Angga Saputra[1], Mona Sari[2], Aminatun[3], Tri Suciati[4], Che Wan Sharifah Robiah Mohamad[5], Gunawarman[6], Yusril Yusuf[2]

[1]*Department of Physics, Faculty of Mathematics and Natural Sciences, IPB University, Bogor, 16680, Indonesia*
[2]*Department of Physics, Faculty of Mathematics and Natural Sciences, Universitas Gadjah Mada, Yogyakarta, 55281, Indonesia*
[3]*Department of Physics, Faculty of Mathematics and Natural Sciences, Universitas Airlangga, Surabaya, 60115, Indonesia*
[4]*Department of Pharmaceutics, School of Pharmacy, Institut Teknologi Bandung, Bandung, 40132, Indonesia*
[5]*Faculty of Electronic Engineering & Technology, Universiti Malaysia Perlis (UniMAP), Kangar, 02600, Malaysia*
[6]*Department of Mechanical Engineering, Universitas Andalas, Padang, 25163, Indonesia*
*__Corresponding author__: yessie.sari@apps.ipb.ac.id

Abstract
In this study, 3D porous multicomponent bioceramic scaffolds were fabricated. Hydroxyapatite (HA) and carbonate-substituted hydroxyapatite (CHA) synthesized from Asian moon scallop shell (*Amusium pleuronectes*) served as the bioceramics, whereas alginate and chitosan served as the polymeric components. The study was focused on determining whether the presence of polyvinyl alcohol (PVA) in the scaffold exerted an impact. When PVA was not included, the morphological examination revealed that the samples exhibited porous structures characterized by effective pore interconnectivity and a substantial pore size. X-ray diffraction and scanning electron microscopic analyses indicated that the inclusion of PVA led to a decrease in the crystallinity, pore size, and porosity of the scaffolds. Those containing PVA exhibited porosity levels in the range of 56%–60%, and pore sizes ranged from 42 to 90 µm. These properties may provide advantages for the scaffold with respect to the ability for cell migration and cell attachment, thus enhancing new bone formation. Moreover, the compositions of HA and chemically modified HA (CHA) within the scaffold influenced the crystallinity and uniformity of the scaffold morphology. This finding suggests the potential for crafting a customized porous bioceramic scaffold based on specific compositions.

Keywords
Biomaterials, Bone Tissue, Carbonate-Substitute Hydroxyapatite, Hydroxyapatite, Porosity

Received: 29 September 2023, Accepted: 6 February 2024
https://doi.org/10.26554/sti.2024.9.2.235-243

1. INTRODUCTION

The primary methods employed in bone reconstruction and repair are bone grafts and artificial scaffolds (Sallent et al., 2020). Utilizing other part of a patient's body is commonly opted for the bone graft technique. Although autografts demonstrate osteoinduction, osteoconduction, and osteogenic capabilities, they may lead to donor tissue morbidity. An alternative is allografts, which use bones from other individuals, posing a risk of rejection by the recipient's body. Xenografts involve the use of bones from other species and are also associated with the risk of rejection. These limitations of autografts, allografts, and xenografts highlight the need for synthetic materials as alternatives in bone grafting procedures. A commonly used artificial material for bone grafts belongs to calcium phosphate, which is a ceramic. Hydroxyapatite (HA) is the ceramic commonly observed in the bone tissue. Stoichiometrically, HA has chemical formula of $Ca_{10}(PO_4)_6(OH)_2$. The natural process of bone mineralization is a complex phenomenon that involves intricate interactions of ions, stereochemistry, and structure, which occur at the interface between biomacromolecules and minerals (Murphy and Mooney, 2002). Ionic interaction in bone mineralization encompasses the process of ionic substitution within HA, which leads to the formation of a nonstoichiometric HA. One prominent phenomenon during bone mineralization is carbonate substitution, which gives rise to carbonate-substituted hydroxyapatite (CHA) (Ishikawa and Hayashi, 2021; Weiner and Traub, 1992). In biological systems, bone minerals encompass carbonate ions in the range of 2%–8% (Gibson and Bonfield, 2002). Diverse techniques, such as ultrasound-assisted sol-gel (Phatai et al., 2018), electrolysis (Supriyono et al., 2023), microwave-assisted hydrothermal technique (Yu et al., 2018), and microwave-assisted precipitation methods (Sari et al., 2021c), have been devised to enable the swift and effective production of synthetic HA. To repli-

cate the natural occurance of bone mineral, carbonate ions have been intentionally integrated into the synthesis process of chemically modified HA (CHA) (Sari et al., 2021a; Sari et al., 2021b; Siddiqi and Azhar, 2020; Pebriani and Sari, 2019; Asra et al., 2018). HA and CHA are widely applied in the medical device field as bone grafts and coating biomaterials (Ningrum et al., 2023; Dewi et al., 2020). The bone scaffold is as crucial as synthetic bone minerals with respect to bone reconstruction and repair. A bone scaffold functions as a three-dimensional (3D) matrix that facilitates and enhances the attachment and proliferation of osteoinductive cells on its surfaces (Sallent et al., 2020). In the living body, this scaffold is formed by collagen, with calcium phosphate being the bone mineral distributed throughout the collagen (Mondal and Pal, 2019). Biomimetic bone formation is mediated by the presence of pores in the collagen. Therefore, the inclusion of porosity in artificial bone scaffolds is essential to promote the colonization of bone cells. Natural polymers, such as gelatin, fibrin, starch, and chitosan, hold potential as artificial bone scaffolds. The inherent characteristics of these polymers provide benefits such as high biocompatibility and osteoconductivity (Rahman et al., 2018). Additionally, reports have been published on the utilization of combined natural and synthetic polymers as scaffold materials to enhance the biocompatibility as well as the capacity to load cells (Zhang et al., 2019; Tripathy et al., 2019). Various synthetic biodegradable polymers, including polylactic-co-glycolic acid, polyethylene glycol, poly-l-lactic acid, polycaprolactone, and poly vinyl alcohol (PVA), have been examined for their suitability in bone tissue engineering. The advantage of using natural or synthetic biodegradable polymers in bone scaffolds lies in their ability to act as a template for the attachment of bone-forming cells, thus permitting cell differentiation into bone. Following biomimetic bone formation, the polymeric scaffold degrades, which is conducive for the healing process (Aoki and Saito, 2020). Recent reviews have emphasized the significant potential of 3D scaffold biomaterials in patients with bone cancer owing to their ability to offer dual efficacy in both tissue regeneration and cancer treatment. However, certain studies have suggested that 3D bioceramic scaffolds composed of a single component may not be ideal owing to various factors. These include challenges such as difficulty in inducing angiogenesis, low efficiency for bone formation, limitations in treating tumors, and susceptibility to bacterial growth. These identified issues pose obstacles for the optimal development of bioceramic scaffolds. Consequently, there is a growing demand for multicomponent bioceramics as a strategy to overcome these challenges and enhance the overall performance of scaffolds in the context of tissue engineering and cancer treatment (Liu et al., 2023; Ma et al., 2023). For this purpose, multicomponent bioceramics have been developed. In this study, a 3D porous multicomponent bioceramic scaffold comprising HA/CHA and polymers was synthesized. The effect of the co-presence of HA and CHA in the scaffold was investigated. Furthermore, the presence of PVA in the scaffold was evaluated. This study was focused on crystallography and morphological effects. Investigation was conducted based on data obtained from X-ray diffraction (XRD) and scanning electron microscopy (SEM).

2. EXPERIMENTAL SECTION

2.1 Materials

For the synthesis of HA and CHA bioceramics, the Asian moon scallop shell (*Amusium pleuronectes*) was employed as the calcium biogenic source. Precursors, such as phosphoric acid (H_3PO_4), diammonium hydrogen phosphate ($(NH_4)_2HPO_4$), ammonium bicarbonate (NH_4HCO_3), and ammonium hydroxide (NH_4OH) 25% solution, were purchased from Merck and used for the synthesis of HA and CHA. Calcium phosphates were synthesized using the precipitation and microwave methods (Sari et al., 2021c; Syafaat and Yusuf, 2019). Chitosan of medium molecular weight (Aldrich, CAS No. 9012-76-4), sodium alginate (Aldrich, CAS No. 9005-38-3), PVA (Aldrich, CAS No. 9002-89-5), NaOH (Aldrich), $CaCl_2$ pro analyze (Aldrich), acetic acid, and distilled water (aquadest) were employed as the materials for fabricating the scaffold.

2.2 Experimental Design: Polymer to HA/CHA Ratio

In this study, we utilized alginate, chitosan, and PVA polimers for the bone scaffold. The scaffold was designed with a polymer to bioceramic ratio of 75:25 wt%. Alginate, one of the scaffold polymers, was consistently maintained at 12.5 wt% (the weight of alginate relative to the total weight of polymers and the bioceramic). PVA was introduced to replace 25% of the chitosan. Consequently, the chitosan content accounted for 62.5 wt% and 46.875 wt% (the weight of chitosan relative to the total weight of polymers and the bioceramic) for samples without PVA (NP) and with PVA (WP), respectively (Table 1). Additionally, the ratio of bioceramics, specifically CHA to HA, was varied for each sample group.

Table 1. The Experimental Design of Scaffolds of HA/CHA with and without PVA

Sample Code	Polymer (% wt)			Bioceramic (%wt)	
	PVA	Chitosan	Alginate	CHA	HA
NP1	-	62.5	12.5	25	0
NP2	-	62.5	12.5	18.75	6.25
NP3	-	62.5	12.5	12.50	12.50
NP4	-	62.5	12.5	6.25	18.75
NP5	-	62.5	12.5	0	25
WP1	15.625	46.875	12.5	25	0
WP2	15.625	46.875	12.5	18.75	6.25
WP3	15.625	46.875	12.5	12.50	12.50
WP4	15.625	46.875	12.5	6.25	18.75
WP5	15.625	46.875	12.5	0	25

2.3 Preparation of the Polymeric Solution

The polymeric solution was formulated by preparing 30% (wt/v) alginate solution in distilled water. For homogenization, the alginate solution was stirred at ambient temperature

for 1 h. The process for preparing the alginate solution included dissolving 15 g of alginate powder in 50 mL of distilled water. The resulting alginate solution was stirred with a magnetic stirrer for 1 hour at room temperature. Subsequently, for preparing the chitosan solution, 2% (v/v) acidic solution was initially prepared. For this, 2 mL of pure acetic acid was dissolved in 100 mL of distilled water. Next, 1 g of chitosan was added to it. The solution was homogenized by stirring it for 1 h at ambient temperature. The PVA solution was formulated by dissolving 5 g of PVA powder in 50 mL of distilled water. The solution was stirred with a magnetic stirrer at a temperature of approximately 85°C for a duration of approximately 3 h until a uniform and homogeneous solution was achieved.

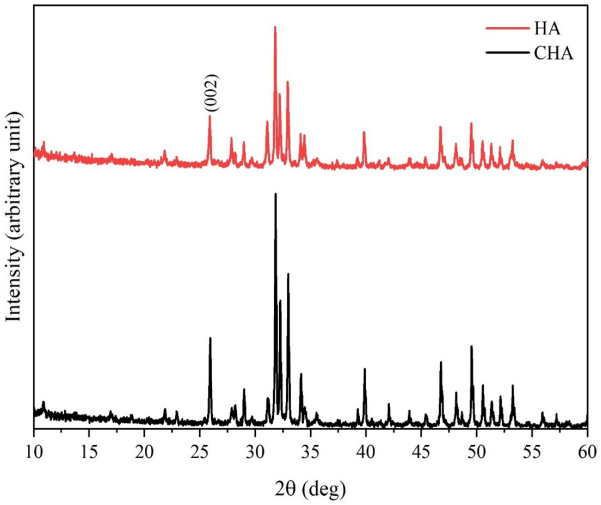

Figure 1. XRD Patterns of HA and CHA

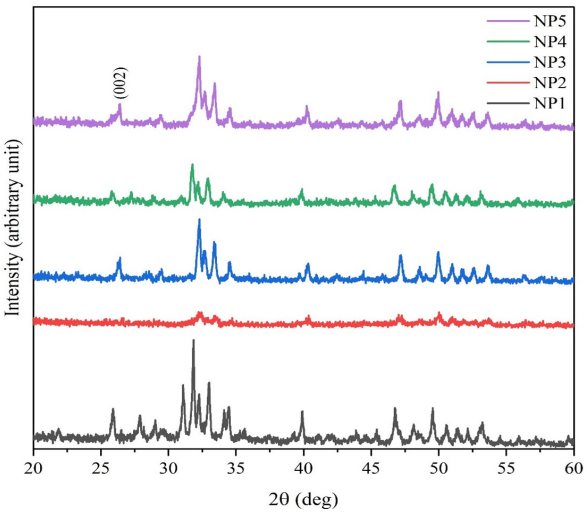

Figure 2. XRD Patterns of Scaffolds without PVA: NP

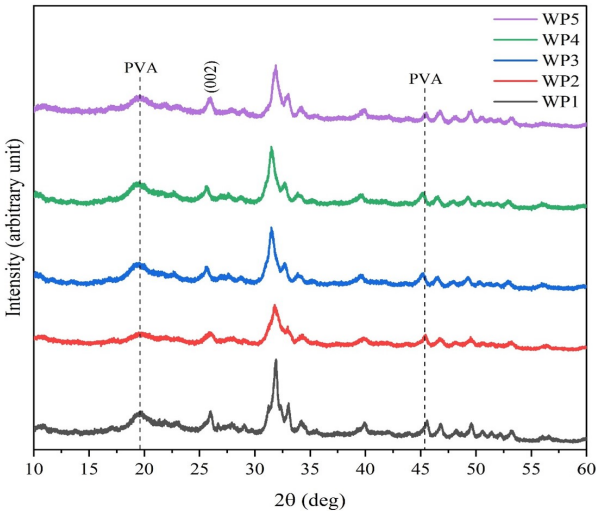

Figure 3. XRD Patterns of Scaffolds with PVA: WP

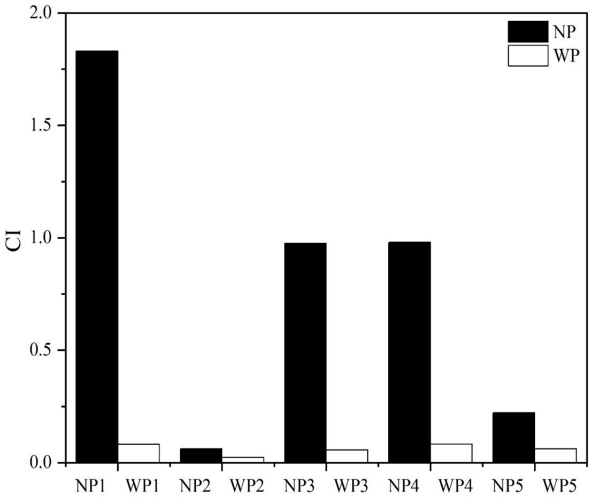

Figure 4. The Crystallinity of the Scaffold at Different Scaffold-Graft Ratio

2.4 Synthesis and Characterization of the Scaffold

In the synthesis process, the chitosan solution was meticulously introduced into the alginate solution, and the resulting mixture was stirred for 30 min. Subsequently, HA and CHA were added, and the scaffold solution was stirred for an additional 60 min. A solution of 1 N NaOH (0.2 mL) was then introduced, followed by the addition of 1 mL of 0.2 M $CaCl_2$ as the crosslinker. The mixture was stirred for an additional 30 min. The resultant scaffold solution was poured into a 24-multiwell plate and stored at -4°C overnight. The last stage included freeze-drying to create the final 3D scaffold. For the sample containing PVA, this solution was added to the mixture of chitosan and alginate before the addition of HA and CHA. The subsequent steps of the synthesis process remained the

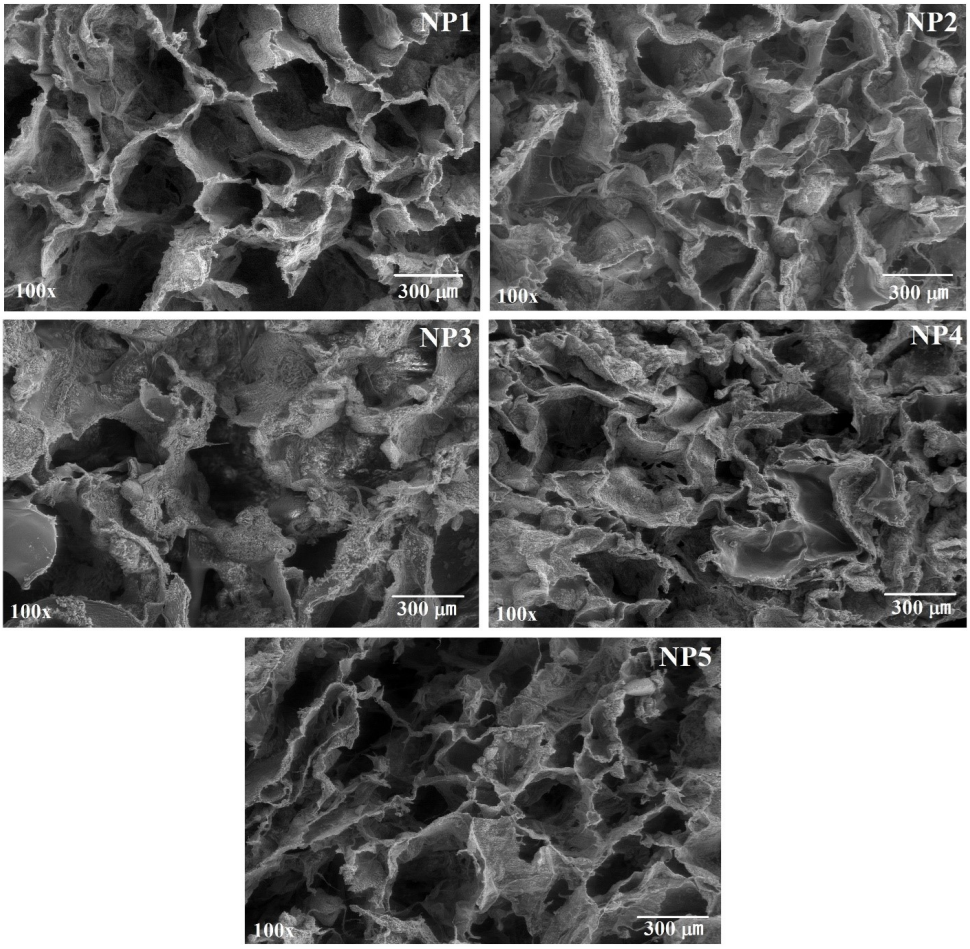

Figure 5. SEM Images of the Scaffold without PVA

same. The scaffold was characterized using XRD to identify the phases present in the material. The examination was performed using the PAN analytical instrument, specifically the Empyrean type, which was outfitted with a Cu-Kα source (λ = 1.54187 Å). The 2θ angle range was set between 10 and 60 degrees, with a functional voltage of 40 kV and a current of 30 mA. The XRD results were depicted in the form of phase graphs, and the phases were discerned by analyzing the diffraction angle and intensity. Specific phases were identified in accordance with the guidelines of the Joint Committee on Powder Diffraction Standards. The crystallinity index (CI) of the scaffold was determined using OriginLab and was computed as the ratio of the area of the crystalline peak to the total area encompassing both crystalline and amorphous regions. SEM analysis was employed to determine the surface morphology and pore size of the scaffolds. The characterization was performed using a JEOL type JSM-6510LA instrument. Prior to imaging, the scaffold surfaces were coated with gold (Au). Images were generated using electron scattering, which were subsequently analyzed. Data related to pore size and porosity were extracted via image processing using the ImageJ software. This method enabled the detailed examination of the structural features of the scaffold and provided quantitative information on pore characteristics.

3. RESULTS AND DISCUSSION

3.1 XRD Analysis of HA and CHA

Figure 1 displays the XRD profiles of HA and CHA utilized in this study. CHA was incorporated in the scaffold owing to its high presence in the human bone (Asra et al., 2018; Soejoko et al., 2014). Both HA and CHA belong to the calcium phosphate class. HA is stoichiometrically represented as ($Ca_{10}(PO_4)_6(OH)_2$). In CHA, carbonate is incorporated in the HA structure and may replace phosphate or hydroxyl groups. As both HA and CHA shared high similarity in chemical composition, their XRD patterns (as shown in Figure 1) were analogous, which posed challenges in differentiating individual peaks of HA and CHA. The success of HA and CHA synthesis was confirmed via lattice parameter evaluation. This analysis (Table 2) confirmed the presence of HA and CHA in each sample. Differentiation between HA and CHA was possible based on their lattice parameters, with CHA exhibiting

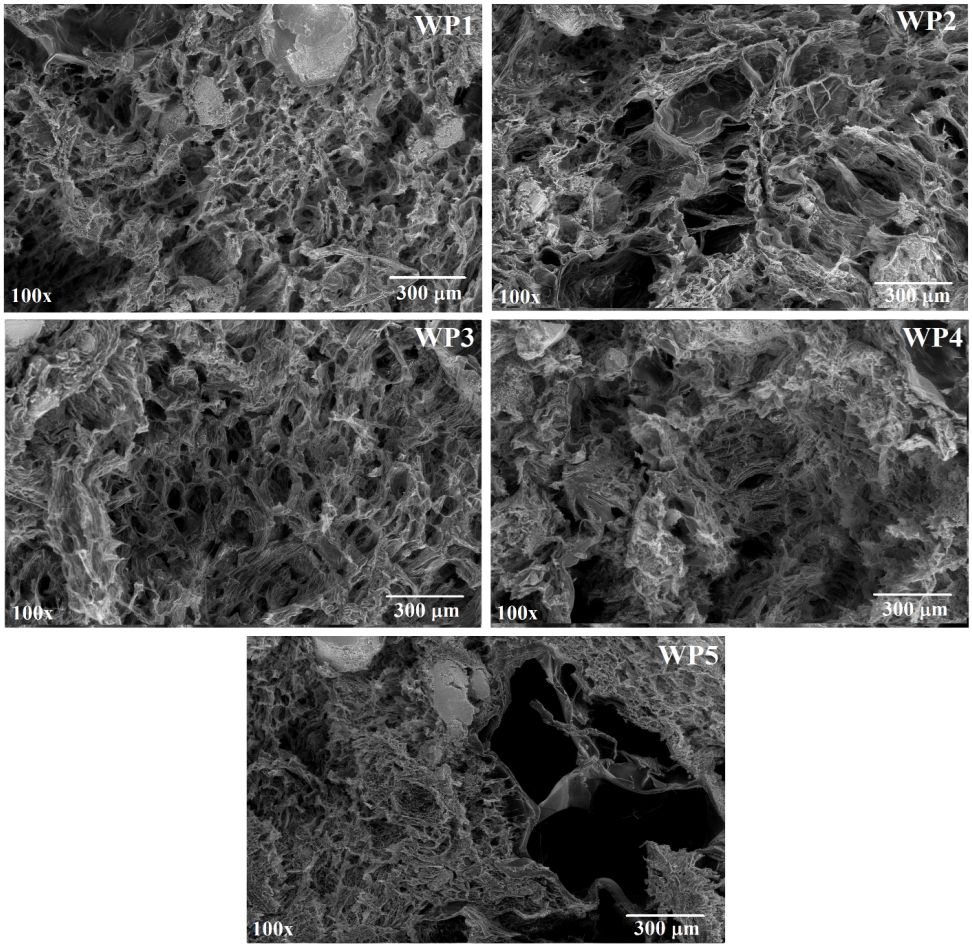

Figure 6. SEM Images of the Scaffold with PVA

lower lattice parameters (a = b) than HA owing to carbonate substitution.

3.2 Effect of PVA-HA/CHA Ratio on the Crystallinity

In this study, a composite was constructed as the 3D scaffold using HA and CHA and a mixture of polymers. The polymers served as the matrix, while the HA/CHA acted as the filler. The matrix had a weight percentage of 70%, while the filler had a weight percentage of 30%. Furthermore, the effect of PVA as a part of the matrix components was investigated (See Table 1). Figures 2 and 3 present the XRD patterns of the scaffolds without and with PVA, respectively. The presence of PVA was identified by the appearance of peaks at 2θ angles around 20° and 45°, which corresponded to the characteristic peaks of PVA (Shuai et al., 2013). The XRD patterns of samples with PVA (WP) exhibited broadening of the full width at half maximum, particularly in the 2θ angle range of 25°–35°, as compared with samples that lacked PVA (Figure 2). This broadening indicates a reduction in crystallinity of the scaffolds in the presence of PVA. Quantification of crystallinity via CI calculation (Table 3) further supported the finding that the composition of the scaffold influenced the CI. The addition of PVA was found to decrease the crystallinity of the scaffold. This result is aligned with a previous study that fabricated a scaffold comprising PVA, nanoHA, and cellulose nanocrystals, which also reported a reduction in crystallinity upon the incorporation of PVA (Kumar et al., 2014). The presence of PVA highly affected the scaffold crystallinity. The introduction of PVA resulted in the decrease of crystallinity (Figure 4). This result signifies that the scaffold with PVA may be advantageous in bone tissue engineering. A study on the effect of scaffold (poly lactide-co-glycolide/apatite) crystallinity on bone formation indicated that the scaffold with lower crystallinity provided better attachment for osteoblast-like cells and thus enhanced new bone formation (Hayakawa et al., 2009). Our findings indicated that the graft type also had an impact on the crystallinity of the scaffolds. The HA and CHA synthesized in this study exhibited different CIs, as shown in Table 3. CHA demonstrated a slightly higher crystallinity than HA. Consequently, scaffolds containing only CHA (samples with an index of "1") had a higher CI than those containing only HA (samples with an index of "5"). This difference in crystallinity between HA and

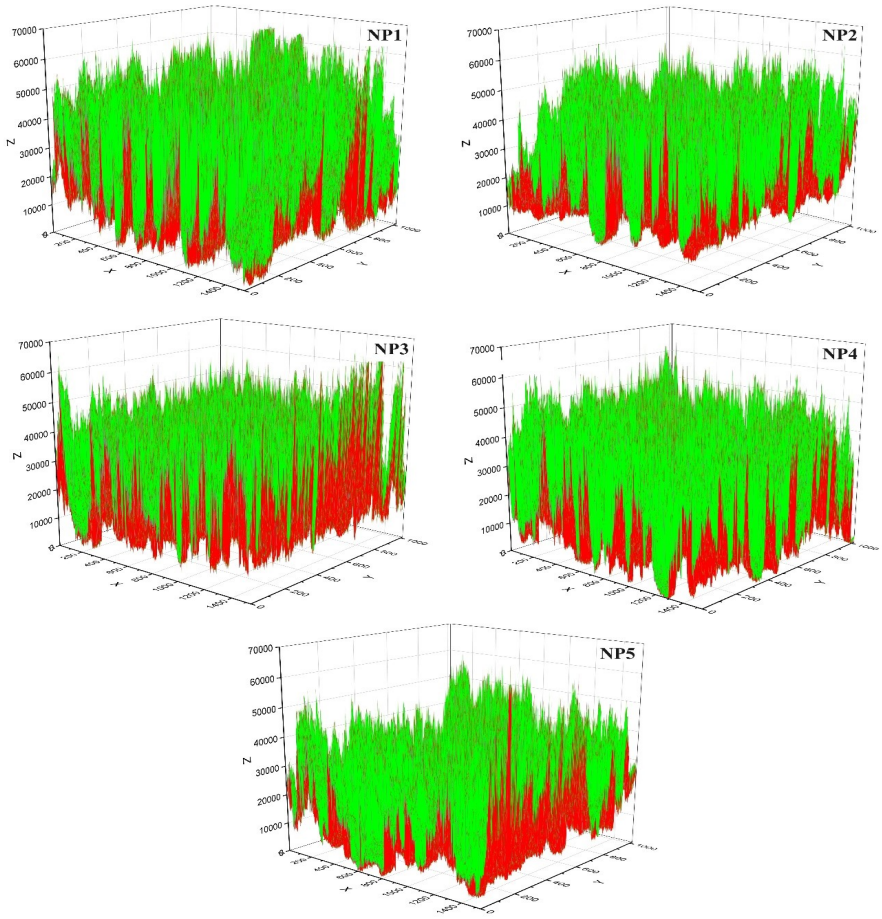

Figure 7. The 3D Plot Surface Area of the Scaffold without PVA

CHA can influence the overall crystallinity of the composite scaffolds, which highlights the significance of the graft type in determining the structural properties of the synthesized materials. Moreover, samples having 18.75 wt% CHA/6.25 wt% HA without or with PVA (NP2 or WP2, respectively) exhibited the lowest CI in the group. These observations on the influences of PVA and HA/CHA ratio on the crystallinity of the scaffold suggest that using PVA and a mixture of HA/CHA is advantageous and can aid in the synthesis of a low crystallinity scaffold. Under this condition, hypothetically, new bone formation will be enhanced. To confirm this hypothesis, in vitro and in vivo studies are required.

3.3 Effect of PVA-HA/CHA Ratio on the Pore Size and Porosity

Scaffold has functions as both providing structural functionality and supporting the biological process. To support the last function, the presence of a porous matrix is mandatory. Porosity of scaffolds is essential for facilitating cell migration and promoting nutrient supply, both of which are critical aspects in tissue engineering and regenerative medicine. The porous structure permits the infiltration of cells, nutrients, and other bioactive factors, fostering a conducive environment for tissue regeneration and integration. Therefore, the design and optimization of porous matrices in scaffolds play a pivotal role in their effectiveness for various biomedical applications (Maheshwari et al., 2014). Figure 5 presents the SEM images of scaffolds without PVA, which reveals the formation of interconnected pores across all samples. The interconnected pore structure is a positive feature of scaffolds in tissue engineering applications as it permits the effective infiltration of cells, nutrients, and other bioactive components, supporting tissue regeneration and integration. The SEM images provide visual evidence for the porous nature of the scaffolds, indicating their potential suitability for facilitating biological processes in the context of tissue engineering. These features were also observed in scaffolds with PVA (Figure 6). However, these samples had a smaller pore size than scaffolds without PVA. Furthermore, the porosity calculation supported this finding. In addition to reducing the pore size and porosity, the presence of PVA improved the mechanical property of the scaffolds. The scaffolds with PVA were physically observed to be less fragile than those

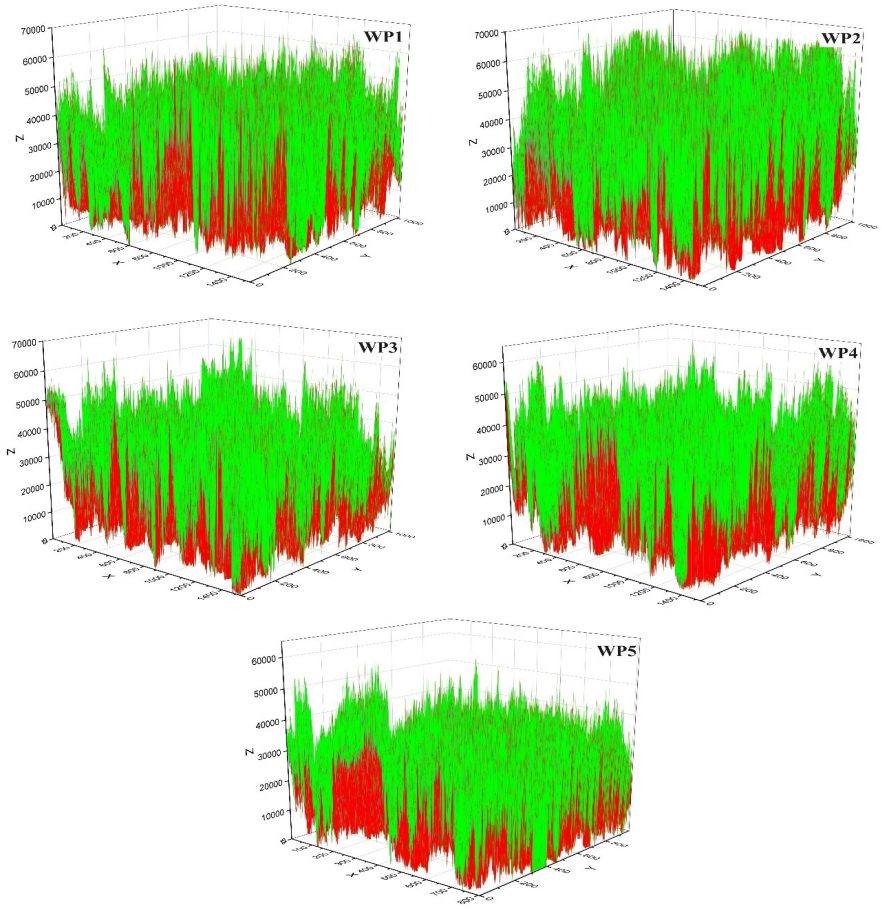

Figure 8. The 3D Plot Surface Area of the Scaffold with PVA

Table 2. Lattice Parameters Data

Sample	Lattice Parameters			
	a = b (Å)	accuracy (%)	c (Å)	accuracy (%)
HA: PDF#09-0432	9.418		6.884	
HA obtained in this study	9.435	99.82	6.883	99.99
CHA: PDF#19-0272	9.309		6.927	
CHA obtained in this study	9.369	99.36	6.840	98.74

without PVA. Quantitative mechanical analysis is therefore advised in future investigations. The scaffolds without PVA exhibited a pore size of 85.8–189.8 µm, whereas those with PVA had a narrower range of 42.5–62.5 µm. Pore size is a critical parameter of scaffolds as it influences cell and nutrient transport, scaffold structural stability, and cell adherence to the scaffold surface. Excessively large pores may facilitate cell and nutrient transport but could compromise scaffold structural stability. Conversely, overly small pores may impede cell and nutrient movement. To ensure cell migration and adhesion to the scaffold, an appropriate pore size is necessary. The observed pore sizes in the range of 50–1000 µm for all samples are aligned with reported suitable ranges for cell growth on scaffolds (Zhao et al., 2018). However, it is important to note that smaller pore sizes can contribute to enhanced scaffold mechanical strength. The balance between pore size and mechanical strength is crucial in designing scaffolds that meet the structural and biological requirements for successful tissue engineering applications (Zhao et al., 2018). Both scaffolds with and without PVA had porosity >50%. Hence, the scaffolds may be advantageous for the adherence and proliferation of cells (Maheshwari et al., 2014). Data obtained from SEM

Table 3. Crystallinity Index, Porosity, and Pore Size of the Scaffold

Sample	CI XRD*	Porosity (%)	Pore Size(µm)
HA	8.3605 ± 0.0150	n.a	n.a
CHA	9.2454 ± 0.0172	n.a	n.a
NP1	1.8304 ± 0.0000	62.56 ± 0.75	189.78 ± 34.5
NP2	0.0613 ± 0.0000	60.94 ± 2.15	125.45 ± 26.89
NP3	0.9748 ± 0.0009	55.74 ± 0.12	106.62 ± 24.1
NP4	0.9790 ± 0.0000	55.81 ± 0.91	97.47 ± 24.12
NP5	0.2421 ± 0.0005	62.09 ± 0.47	83.56 ± 5.34
WP1	0.0810 ± 0.0000	57.25 ± 2.06	45.90 ± 4.3
WP2	0.0239 ± 0.0000	60.22 ± 1.57	62.55 ± 15.67
WP3	0.0568 ± 0.0000	57.85 ± 1.38	43.99 ± 3.46
WP4	0.0821 ± 0.0000	60.85 ± 1.22	42.44 ± 6.10
WP5	0.0610 ± 0.0000	56.04 ± 0.13	42.50 ± 9.29

*n.a: not available

analysis from scaffold with and without PVA was further processed with OriginLab to obtain the 3D surface area (Figures 7 and 8, respectively). In these visual representations, the solid particles (polymers and bioceramics) distribution is colored in green, while the pore is in red. Overall, the incorporation of PVA appears to enhance the even distribution of both solid particles and pores. Observations drawn from the 3D surface area plots reveal that samples WP2 and WP3 demonstrate the highest uniformity in the distribution of both solid particles and pores. This characteristic holds potential for enhancing cellular activities. Nevertheless, it is vital to emphasize that additional studies, particularly in vitro investigations, are essential to validate this hypothesis. The 3D surface area plots offer visual insights into the distribution patterns of solid particles and pores, indicating potential enhancements in the presence of PVA.

4. CONCLUSION

This research explored the potential of HA/CHA and polymeric scaffolds as 3D porous multicomponent bioceramic scaffolds. HA and CHA were successfully synthesized from biogenic resources (Asian moon scallop shell) with and without the presence of PVA. XRD and SEM analyses were performed to assess the influence of PVA addition and HA/CHA composition on the scaffolds. The findings indicated that alginate and chitosan could serve as scaffolds with an interconnected porous structure. Furthermore, introducing PVA into the polymer component enhanced the mechanical properties of the scaffolds, rendering them less brittle. However, this improvement was accompanied by a decrease in crystallinity, porosity, and pore size. Scaffolds incorporating PVA displayed porosity in the range of 56%–60% and pore size in the range of 42–90 µm. With these characteristics, along with low crystallinity, scaffolds containing PVA demonstrated promising potential as candidates for bone tissue engineering. The 3D surface plot analysis indicated that scaffolds with PVA exhibited a more homogeneous surface area, particularly in samples WP2 and WP3, where both HA and CHA were present in the scaffold. However, further in vitro studies are needed to validate these observations.

5. ACKNOWLEDGMENT

This research received financial support from the Ministry of Education, Culture, Research, and Technology of the Republic of Indonesia under the Riset Kolaborasi Indonesia – World Class University scheme (796/UN1.DITLIT/DIT-LIT/PT/2021).

REFERENCES

Aoki, K. and N. Saito (2020). Biodegradable Polymers As Drug Delivery Systems for Bone Regeneration. *Pharmaceutics*, **12**(2); 95

Asra, D. Y., Y. W. Sari, and K. Dahlan (2018). Effect of Microwave Irradiation on the Synthesis of Carbonated Hydroxyapatite (CHA) from Chicken Eggshell. In *IOP Conference Series: Earth and Environmental Science*, volume 187. IOP Publishing, page 012016

Dewi, A. H., D. K. Yulianto, I. D. Ana, R. Rochmadi, and W. Siswomihardjo (2020). Effect of Cinnamaldehyde, an Anti-Inflammatory Agent, on the Surface Characteristics of a Plaster of Paris-$CaCO_3$ Hydrogel for Bone Substitution in Biomedicine. *International Journal of Technology*, **11**(5); 963–973

Gibson, I. R. and W. Bonfield (2002). Novel Synthesis and Characterization of an AB-Type Carbonate-Substituted Hydroxyapatite. *Journal of Biomedical Materials Research*, **59**(4); 697–708

Hayakawa, T., C. Mochizuki, H. Hara, T. Fukushima, F. Yang, H. Shen, S. Wang, and M. Sato (2009). Influence of Apatite Crystallinity in Porous PLGA/apatite Composite Scaffold on Cortical Bone Response. *Journal of Hard Tissue Biology*, **18**(1); 7–12

Ishikawa, K. and K. Hayashi (2021). Carbonate Apatite Artificial Bone. *Science and Technology of Advanced Materials*, **22**(1); 683–694

Kumar, A., Y. S. Negi, V. Choudhary, and N. K. Bhardwaj (2014). Microstructural and Mechanical Properties of Porous Biocomposite Scaffolds Based on Polyvinyl Alcohol, Nano-Hydroxyapatite and Cellulose Nanocrystals. *Cellulose*, **21**; 3409–3426

Liu, X., Y. Liu, L. Qiang, Y. Ren, Y. Lin, H. Li, Q. Chen, S. Gao, X. Yang, and C. Zhang (2023). Multifunctional 3D-Printed Bioceramic Scaffolds: Recent Strategies for Osteosarcoma Treatment. *Journal of Tissue Engineering*, **14**; 20417314231170371

Ma, Y., B. Zhang, H. Sun, D. Liu, Y. Zhu, Q. Zhu, and X. Liu (2023). The Dual Effect of 3D-Printed Biological Scaffolds Composed of Diverse Biomaterials in the Treatment of Bone Tumors. *International Journal of Nanomedicine*, **18**; 293–305

Maheshwari, S. U., V. K. Samuel, and N. Nagiah (2014). Fab-

rication and Evaluation of (PVA/HAp/PCL) Bilayer Composites As Potential Scaffolds for Bone Tissue Regeneration Application. *Ceramics International*, **40**(6); 8469–8477

Mondal, S. and U. Pal (2019). 3D Hydroxyapatite Scaffold for Bone Regeneration and Local Drug Delivery Applications. *Journal of Drug Delivery Science and Technology*, **53**; 101131

Murphy, W. L. and D. J. Mooney (2002). Bioinspired Growth of Crystalline Carbonate Apatite on Biodegradable Polymer Substrata. *Journal of the American Chemical Society*, **124**(9); 1910–1917

Ningrum, E. O., I. Khoiroh, H. I. Nastiti, R. A. Affan, A. D. Karisma, E. Agustiani, A. Surono, H. Suroto, S. Suprapto, and L. S. Taji (2023). Surface Coating Effect on Corrosion Resistance of Titanium Alloy Bone Implants by Anodizing Method. *International Journal of Technology*, **14**(4); 749–760

Pebriani, C. and Y. Sari (2019). Microwave–Assisted Precipitation of Carbonated Hydroxyapatite. In *Journal of Physics: Conference Series*, volume 1248. IOP Publishing, page 012078

Phatai, P., C. M. Futalan, S. Utara, P. Khemthong, and S. Kamonwannasit (2018). Structural Characterization of Cerium-Doped Hydroxyapatite Nanoparticles Synthesized by an Ultrasonic-Assisted Sol-Gel Technique. *Results in Physics*, **10**; 956–963

Rahman, M. M., M. Shahruzzaman, M. S. Islam, M. N. Khan, and P. Haque (2018). Preparation and Properties of Biodegradable Polymer/nano-Hydroxyapatite Bioceramic Scaffold for Spongy Bone Regeneration. *Journal of Polymer Engineering*, **39**(2); 134–142

Sallent, I., H. Capella-Monson'ıs, P. Procter, I. Y. Bozo, R. V. Deev, D. Zubov, R. Vasyliev, G. Perale, G. Pertici, and J. Baker (2020). The Few Who Made It: Commercially and Clinically Successful Innovative Bone Grafts. *Frontiers in Bioengineering and Biotechnology*, **8**; 952

Sari, M., Aminatun, T. Suciati, Y. W. Sari, and Y. Yusuf (2021a). Porous Carbonated Hydroxyapatite-Based Paraffin Wax Nanocomposite Scaffold for Bone Tissue Engineering: A Physicochemical Properties and Cell Viability Assay Analysis. *Coatings*, **11**(10); 1189

Sari, M., P. Hening, I. D. Ana, and Y. Yusuf (2021b). Porous Structure of Bioceramics Carbonated Hydroxyapatite-Based Honeycomb Scaffold for Bone Tissue Engineering. *Materials Today Communications*, **26**; 102135

Sari, Y., A. Saputra, A. Bahtiar, and N. Nuzulia (2021c). Effects of Microwave Processing Parameters on the Properties of Nanohydroxyapatite: Structural, Spectroscopic, Hardness, and Toxicity Studies. *Ceramics International*, **47**(21); 30061–30070

Shuai, C., Z. Mao, H. Lu, Y. Nie, H. Hu, and S. Peng (2013). Fabrication of Porous Polyvinyl Alcohol Scaffold for Bone Tissue Engineering Via Selective Laser Sintering. *Biofabrication*, **5**(1); 015014

Siddiqi, S. A. and U. Azhar (2020). Carbonate Substituted Hydroxyapatite. In *Handbook of Ionic Substituted Hydroxyapatites*. Elsevier, pages 149–173

Soejoko, D. S., Y. W. Sari, S. U. Dewi, N. Nurizati, K. Dahlan, and D. S. Atmadja (2014). Composition of Human Bone Mineral by FTIR and Its Relationship to the Age. *Journal of Medical Physics and Biophysics*, **1**(1); 2–7

Supriyono, S., C. W. Kartikowati, B. Poerwadi, C. Wulandari, L. L. F. Hikma, A. Azzahra, K. Ghanyysyafira, and H. L. Pinastika (2023). The Formation Process of Hydroxyapatite Nanoparticles by Electrolysis and Their Physical Characteristics. *International Journal of Technology*, **14**(2); 330

Syafaat, F. Y. and Y. Yusuf (2019). Influence of Ca/P Concentration on Hydroxyapatite (HAp) from Asian Moon Scallop Shell *(Amusium Pleuronectes)*. *International Journal of Nanoelectronics and Materials*, **12**(3); 357–362

Tripathy, N., E. Perumal, R. Ahmad, J. E. Song, and G. Khang (2019). Hybrid Composite Biomaterials. In *Principles of regenerative medicine*. Elsevier, pages 695–714

Weiner, S. and W. Traub (1992). Bone Structure: From Ångstroms to Microns. *The FASEB journal*, **6**(3); 879–885

Yu, H. P., Y. J. Zhu, and B. Q. Lu (2018). Highly Efficient and Environmentally Friendly Microwave-Assisted Hydrothermal Rapid Synthesis of Ultralong Hydroxyapatite Nanowires. *Ceramics International*, **44**(11); 12352–12356

Zhang, Y., X. Liu, L. Zeng, J. Zhang, J. Zuo, J. Zou, J. Ding, and X. Chen (2019). Polymer Fiber Scaffolds for Bone and Cartilage Tissue Engineering. *Advanced Functional Materials*, **29**(36); 1903279

Zhao, H., L. Li, S. Ding, C. Liu, and J. Ai (2018). Effect of Porous Structure and Pore Size on Mechanical Strength of 3D-Printed Comby Scaffolds. *Materials letters*, **223**; 21–24

